mathematics

MDPI

Article

Joint Optimization of UAV Communication and Time-Constrained Pickup Missions

Jun-Pyo Hong

School of Electronics and Electrical Engineering, Hongik University, Seoul 04066, Republic of Korea; jp_hong@hongik.ac.kr

Abstract

Unmanned aerial vehicles (UAVs) are increasingly expected to support both wireless communication and logistics missions, creating a need for integrated operation strategies that jointly manage data collection and physical item handling. This paper investigates a UAV system that simultaneously performs uplink communication with multiple ground nodes (GNs) while completing time-constrained item-pickup tasks. To enhance both throughput and fairness across GNs, we maximize the proportional fair spectral efficiency of GNs while ensuring that all items are collected within the required mission duration under payload and geographical constraints. The resulting formulation constitutes a mixed-integer nonconvex optimization problem involving binary pickup assignments, binary communication scheduling, and trajectory-dependent channel coupling, making direct global optimization intractable. To address this challenge, we develop an iterative convexification framework that integrates the successive convex approximation and the penalty convex–concave procedure within a block coordinate descent structure, enabling efficient joint optimization of trajectory, pickup timing/sequence, and GN scheduling. Simulation results validate that the proposed scheme dynamically shapes the UAV trajectory to improve channel conditions without violating the pickup deadline and compensates disadvantaged GNs through proportional fair scheduling. As a result, it consistently outperforms the baseline strategies under various system parameters.

Keywords: convex optimization; unmanned aerial vehicle; proportional fairness; item pickup; communication

MSC: 90C30

Check for updates

Academic Editors: Ran Sun and Chengxi Zhang

Received: 18 April 2026
Revised: 21 May 2026
Accepted: 21 May 2026
Published: 24 May 2026

Copyright: © 2026 by the author. Licensee MDPI, Basel, Switzerland. This article is an open access article distributed under the terms and conditions of the Creative Commons Attribution (CC BY) license.

1. Introduction

Unmanned aerial vehicles (UAVs) have emerged as a promising technology for next-generation logistics and wireless communication systems due to their high mobility, flexible deployment, and broad service coverage [1,2]. UAV-enabled communication has been widely investigated for a variety of application domains, including wireless-powered networks, secure communication, energy-aware networking, cooperative computing, and UAV-assisted 5G/6G connectivity. In particular, uplink-oriented UAV communication serves as an effective supplementary solution in disaster-stricken or rural areas with limited infrastructure, as well as in temporary hotspots where a sudden surge of traffic must be accommodated without deploying additional fixed base stations [3–5]. At the same time, UAVs are increasingly being adopted as autonomous delivery platforms capable of performing complex logistics tasks such as parcel pickup and transportation, time-critical

dispatching, and large-scale routing for multi-item delivery missions. These two emerging fields, UAV communication and UAV-enabled logistics, are rapidly converging, giving rise to integrated UAV systems that must support both communication service and physical item-handling missions. In addition to communication and logistics design, recent studies have also investigated simulation techniques for complex multiphase-flow phenomena, such as bubbly-flow signal fluctuations under low-void-fraction conditions [6].

However, most existing studies consider these functions separately, assuming either communication-only UAV operation [7–16] or logistics-only delivery tasks [17–21]. Regarding the communication-oriented works, prior research has mainly focused on enhancing wireless performance: some studies have pursued throughput-driven UAV trajectory and communication design [7,8], others have explored energy-aware UAV communication that minimizes propulsion or completion energy [9,10], and several works have jointly considered communication and wireless energy harvesting to simultaneously maintain data transfer and energy replenishment [11–13]. More recently, blockage-aware channel models have also been incorporated into multi-UAV trajectory and resource allocation problems using block successive convex approximation (SCA) techniques [14]. In addition, another research direction addresses secure UAV communication, where UAV mobility and resource allocation are exploited to suppress eavesdropping risks at the physical layer [15,16]. Regarding the logistics-oriented studies, existing works have primarily focused on improving the efficiency of UAV-based delivery missions. Early studies formulated UAV delivery as a vehicle-routing problem to minimize overall travel distance and mission time [17], whereas more recent work has examined stochastic task scheduling for intelligent on-demand delivery services [18]. A separate line of research has optimized UAV trajectory and pickup planning under realistic operational constraints, such as payload limits, no-fly zones, and three-dimensional routing, to reduce delivery time and improve logistical feasibility [19,20]. Moreover, UAV logistics has been extended to swarm-based delivery platforms, in which coordination among multiple UAVs is optimized to enhance scalability and service efficiency [21]. Table 1 summarizes representative UAV-related studies in terms of communication, logistics, time and payload constraints, and optimization objective.

Table 1. Comparison with representative UAV-related studies.

Work	Comm.	Logistics	Time Const.	Payload Const.	Objective
[7]	✓	–	–	–	Throughput
[8]	✓	–	–	–	Throughput
[9]	✓	–	–	–	Energy
[10]	✓	–	✓	–	Completion time
[11]	✓	–	–	–	Throughput
[12]	✓	–	–	–	Throughput
[13]	✓	–	–	–	Throughput
[14]	✓	–	–	–	Throughput
[15]	✓	–	–	–	Secrecy
[16]	✓	–	–	–	Secrecy
[17]	–	✓	✓	✓	Cost/Time
[18]	–	✓	✓	–	Tardiness
[19]	–	✓	–	✓	Completion time
[20]	–	✓	–	✓	Profit
[21]	–	✓	–	✓	Distance
Proposed	✓	✓	✓	✓	PF-SE

Note: "✓" indicates that the corresponding feature is considered, whereas "–" indicates that it is not considered.

In practice, a UAV responsible for both data collection and item pickup must determine how to balance its trajectory, scheduling, and operational timing to satisfy both objectives.

This gives rise to a fundamentally new challenge: how to jointly optimize communication efficiency and time-constrained pickup missions while accommodating stringent payload and safety constraints. The problem becomes even more complex because a UAV serving multiple ground nodes (GNs) must dynamically allocate uplink scheduling while physically visiting designated pickup zones within a limited time window. These dual requirements inherently couple the resource allocation, pickup scheduling, and spatial trajectory design, making the overall decision-making problem highly nonlinear and combinatorial. To address this challenge, this paper investigates a UAV system that simultaneously collects data from multiple GNs while performing time-constrained item-pickup missions. The objective is to maximize the proportional fair (PF) uplink spectral efficiency (SE) of all GNs, thereby improving both throughput and user fairness, while guaranteeing the pickup of all items within the required mission duration. The joint optimization involves binary pickup assignments, binary scheduling indicators, nonconvex spatial constraints, and a nonlinear utility function, resulting in a mixed-integer nonlinear programming (MINLP) that is mathematically intractable to solve directly. To overcome these difficulties, we develop a block-coordinate iterative convexification framework that integrates the SCA and the penalty convex–concave procedure (PCCP). The proposed method converts the original nonconvex problem into a sequence of tractable convex subproblems that can be solved efficiently using standard convex solvers, while progressively enforcing the binary feasibility of pickup and scheduling decisions. This allows the UAV to autonomously coordinate its three-dimensional (3D) trajectory, pickup timing/sequence, and GN scheduling so that both communication and logistics missions can be completed effectively within the given time horizon. Simulation results demonstrate the benefits of the proposed approach. The UAV dynamically bends its trajectory toward GNs to exploit favorable channel conditions while still finishing item pickups on time, and compensates for disadvantaged GNs through PF scheduling. Compared with the baseline strategies, the proposed method shows consistent performance gains under various system parameters. It should be emphasized that the main novelty of this work lies in the integrated problem formulation rather than in the development of a new generic optimization algorithm. While SCA, PCCP, and block-coordinate updates are established optimization tools, they are tailored here to handle the coupled communication scheduling, pickup assignment, payload evolution, altitude control, and trajectory constraints in the proposed MINLP formulation.

The remainder of this paper is organized as follows. Section 2 describes the system model and formulates the optimization problem. Section 3 develops the proposed joint trajectory–pickup–scheduling optimization algorithm. Section 4 evaluates its performance through simulations and comparisons with baseline schemes. Section 5 concludes the paper.

2. System Model and Problem Statement

Figure 1 depicts a system model of UAV communication with time-constrained pickup missions, where a rotary-wing UAV collects data from L GNs, indexed by $l \in \mathcal{L} = \{1, 2, \ldots, L\}$, while also picking up K items at corresponding pickup zones, indexed by $k \in \mathcal{K} = \{1, 2, \ldots, K\}$. The total flight duration T is uniformly divided into N time slots of fixed length $\delta = \frac{T}{N}$, during which the UAV's position is assumed to remain approximately constant owing to the small slot interval [7]. Uplink communication between the UAV and the GNs follows a time-division multiple-access protocol, enabling the UAV to dynamically adjust its position toward the scheduled GN. We assume that the UAV and each GN are equipped with a single omnidirectional antenna.

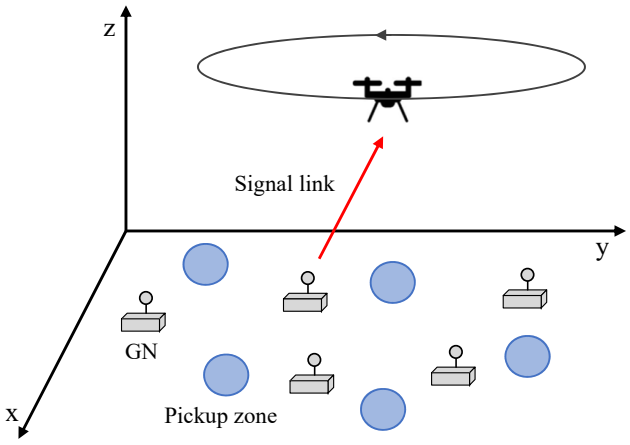


Figure 1. System model of UAV communication with time-constrained pickup missions.

The 3D coordinates of the UAV at time slot $n \in \mathcal{N} = \{1, 2, \ldots, N\}$ are represented by $\mathbf{c}[n] = (\mathbf{q}[n], z[n])$, where $\mathbf{q}[n] = (x[n], y[n])$ and $z[n]$ denote its horizontal and vertical coordinates, respectively. The UAV departs from the origin $\mathbf{c}^{\text{org}}$ and must reach the destination $\mathbf{c}^{\text{dst}}$ by the end of the operation cycle. The UAV's motion is also subject to a maximum velocity constraint $V_{\max}$, which limits the distance traveled during any time slot to within $\delta V_{\max}$. Consequently, the UAV's mobility constraints can be formulated as follows:

$$\mathbf{c}[0] = \mathbf{c}^{\text{org}}, \ \ \mathbf{c}[N] = \mathbf{c}^{\text{dst}}, \tag{1}$$

$$\|\mathbf{c}[n] - \mathbf{c}[n-1]\| \leq \delta V_{\max}, \ \forall n. \tag{2}$$

Let $\alpha_k[n]$ denote a binary decision variable that represents whether the UAV performs a pickup operation for item k during time slot n. Specifically, $\alpha_k[n] = 1$ if item k is picked up by the UAV in slot n, and $\alpha_k[n] = 0$ otherwise. The pickup scheduling constraints of the UAV are then defined as follows:

$$\alpha_k[n] \in \{0, 1\}, \ \forall k, n, \tag{3}$$

$$\sum_{k=1}^{K} \sum_{n=1}^{N_{\text{req}}} \alpha_k[n] \geq K, \tag{4}$$

$$\sum_{n=1}^{N_{\text{req}}} \alpha_k[n] \leq 1, \ \forall k, \tag{5}$$

$$\sum_{k=1}^{K} \alpha_k[n] \leq 1, \ \forall n, \tag{6}$$

$$W[n] = \sum_{k=1}^{K} w_k \left(\sum_{j=1}^{n} \alpha_k[j] \right) \leq W_{\max}, \ \forall n. \tag{7}$$

Constraint (3) defines the binary decision variable $\alpha_k[n]$. Constraint (4) enforces the time constraint, which guarantees that all K items are collected within the required time slot limit N_{req}. Because pickups are only permitted in slots $n \leq N_{\text{req}}$, this condition ensures mission completion before the deadline, thereby satisfying the time-constrained logistics requirement. Constraint (5) ensures that each item can be picked up at most once within the required time slot N_{req}, thereby preventing multiple pickups of the same item. Conversely, (6) restricts the UAV to performing only one pickup per slot, reflecting its physical limitation of handling a single item at a time. Finally, constraint (7) maintains the payload feasibility by ensuring that the cumulative carried weight, given by $W[n]$, never exceeds the UAV's maximum payload capacity $W_{\max}$. Together, these constraints

coordinate the UAV's pickup scheduling, capacity management, and timing to ensure feasible and timely mission execution.

The UAV maintains a constant flight altitude H, with descent below this level permitted solely for executing pickup tasks. The corresponding altitude constraint is therefore formulated as

$$\left(1-\sum_{k=1}^{K}\alpha_k[n]\right)H \le z[n] \le H,\ \forall n. \tag{8}$$

To execute a pickup operation, the UAV must enter and remain within the designated service region of each item. For item k, this region is modeled as a circular zone centered at $\mathbf{c}_k = (\mathbf{q}_k, z_k)$ with radius R_k. These zones define the allowable spatial boundaries within which the UAV can safely approach and complete pickup procedures. The UAV must stay inside the respective zone throughout the pickup process, including during its descent and ascent. Based on this condition, the spatial constraints are formulated as

$$\alpha_k[n]\|\mathbf{c}[n]-\mathbf{c}_k\|^2 \le R_k^2,\ \forall k, n \ne N, \tag{9}$$

$$\alpha_k[n]\|\mathbf{q}[j]-\mathbf{q}_k\|^2 \le R_k^2,\ \forall k, n \ne N, j \in \{n-1, n+1\}. \tag{10}$$

It should be noted that $\alpha_k[n] = 1$ does not imply that the UAV completes the entire approach, descent, pickup, and ascent process within a single slot. By (9), the UAV's 3D position must be inside the pickup region at slot n, which means that the pickup can be executed only when the UAV is located at a feasible pickup position. In addition, by (10), the UAV's horizontal positions at the adjacent slots $n-1$ and $n+1$ must remain within the horizontal boundary of the same pickup region. Therefore, the horizontal approach to the pickup zone is completed before the pickup slot, while the descent and ascent are modeled as local vertical maneuvers around slot n within the pickup boundary. The feasibility of this local maneuver is ensured by the mobility constraint in (2) together with the selected simulation parameters.

For communication operations, let $s_l[n]$ denote a binary scheduling indicator that represents whether GN l is allocated for uplink transmission in time slot n. Specifically, $s_l[n] = 1$ indicates that GN l is scheduled for communication with the UAV during slot n; otherwise, $s_l[n] = 0$. Given that only one GN is served by the UAV per time slot, the following constraints are introduced for the communication scheduling:

$$s_l[n] \in \{0, 1\},\ \forall l, n, \tag{11}$$

$$\sum_{l=1}^{L} s_l[n] \le 1,\ \forall n. \tag{12}$$

Assuming the LoS propagation environment [11–13,15,16], the channel power gain between the UAV and GN l, located at position $\mathbf{c}_l$, during time slot n is given by

$$h_l[n] = \frac{\mu_0}{\|\mathbf{c}[n] - \mathbf{c}_l\|^2},\ \forall l, n, \tag{13}$$

where μ_0 denotes the reference channel gain measured at a distance of 1 m. Under this LoS distance-dependent channel model, the effect of UAV position and altitude during pickup is captured by the trajectory-dependent channel gain. In addition, pickup execution is treated as a local mechanical operation that does not interrupt the UAV's RF receiving module. Therefore, pickup and communication scheduling are not modeled as mutually exclusive operations, and no additional constraint between $\alpha_k[n]$ and $s_l[n]$ is imposed.

Subsequently, the achievable SE between the UAV and GN l at time slot n can be expressed as

$$\begin{aligned} r_l[n] &= \log_2\left(1 + \frac{h_l[n]p_{\text{tx}}}{\sigma^2}\right) \\ &= \log_2\left(1 + \frac{\mu_0 p_{\text{tx}}}{\sigma^2 \|\mathbf{c}[n] - \mathbf{c}_l\|^2}\right), \end{aligned} \tag{14}$$

where p_{tx} denotes the constant transmit power of the GNs, and σ^2 is the noise power. The average SE over the entire flight period can then be represented by

$$R_l = \frac{1}{N}\sum_{n=1}^{N} s_l[n] r_l[n], \ \forall l. \tag{15}$$

To guarantee reliable communication performance for all GNs, a minimum SE requirement is imposed as

$$R_l \geq R_{\min}, \ \forall l, \tag{16}$$

where $R_{\min}$ is the minimum required SE.

In this study, we focus on a proportional-fair resource allocation strategy that enhances both the average SE of GNs and user fairness [22]. Owing to the inherent fairness-promoting property of the logarithmic utility, allocating resources according to this criterion enables balanced SE improvement across all GNs. Therefore, our goal is to maximize the uplink SE in a proportional-fair sense for every GN, while simultaneously guaranteeing that all item-pickup operations are completed within the prescribed time horizon. The optimization is jointly performed over the pickup assignment variables ($\boldsymbol{\alpha} \triangleq \{\alpha_k[n], \forall k, n\}$), the scheduling indicators ($\boldsymbol{s} \triangleq \{s_l[n], \forall l, n\}$), and the UAV trajectory ($\boldsymbol{c} \triangleq \{\mathbf{c}[n], \forall n\}$), which can be formulated as follows:

$$\begin{aligned} \textbf{(P1):} \ \max_{\boldsymbol{s}, \boldsymbol{\alpha}, \boldsymbol{c}} \quad & \sum_{l=1}^{L} \ln(R_l) \\ \text{subject to} \quad & (1) - (12), \ (16). \end{aligned}$$

Problem **(P1)** is the MINLP problem because both the pickup assignment variables $\boldsymbol{\alpha}$ and the scheduling indicators $\boldsymbol{s}$ are binary, as defined in (3) and (11). Moreover, the objective function and constraints (9), (10), and (16) are inherently nonconvex with respect to their associated optimization variables. As a result, obtaining a globally optimal closed-form solution is mathematically intractable, and efficient convexification or approximation techniques are required to derive a high-quality feasible solution.

3. Proposed Optimization Method

To handle the nonconvexity present in problem **(P1)**, an iterative convexification framework combining the SCA and PCCP is adopted within a block coordinate descent algorithm. Through this approach, the original nonconvex problem is successively reformulated into a series of convex subproblems that can be efficiently solved using standard convex optimization tools such as CVX [23]. The detailed procedure of the proposed algorithm is described below.

3.1. Optimization of Scheduling Indicator

Relaxing $s_l[n]$ to be continuous on $[0,1]$, the subproblem of optimizing $\boldsymbol{s}$ for fixed $\boldsymbol{\alpha}$ and $\boldsymbol{c}$ is

$$\begin{aligned} \textbf{(P2-1):} \ \max_{\boldsymbol{s}} \quad & \sum_{l=1}^{L} \ln(R_l) \\ \text{s. t.} \quad & 0 \le s_l[n] \le 1, \ \forall l, n, \\ & (12), \ (16), \end{aligned} \tag{17}$$

which is a standard linear program and can be efficiently solved via CVX. The resulting fractional schedule can be converted to a binary one without loss of optimality using the time-sharing reconstruction in [7].

3.2. Optimization of Pickup Assignment and Trajectory

The subproblem of optimizing $\boldsymbol{\alpha}$ and $\boldsymbol{c}$ for fixed $\boldsymbol{s}$ is given by

$$\begin{aligned} \textbf{(P2-2):} \ \max_{\boldsymbol{\alpha},\, \boldsymbol{c}} \quad & \sum_{l=1}^{L} \ln(R_l) \\ \text{subject to} \quad & (1) - (10), \ (16). \end{aligned}$$

Unlike the scheduling variable $s_l[n]$, which can be relaxed and later reconstructed through time-sharing without performance loss, the pickup assignment variable $\alpha_k[n]$ must strictly satisfy binary feasibility since each item can only be picked up once in a discrete time slot. To handle the binary nature of $\alpha_k[n]$ in (3), it can be equivalently reformulated as

$$\alpha_k[n] \in [0,1], \ \forall k, n, \tag{18}$$

$$\alpha_k[n](1 - \alpha_k[n]) \le 0, \ \forall k, n. \tag{19}$$

In this reformulation, (18) relaxes $\alpha_k[n]$ to a continuous domain, while (19) enforces its binary property. However, the nonlinear constraint in (19) renders the problem nonconvex, and the resulting feasible set becomes highly restricted, thereby increasing the computational difficulty of directly solving the problem. To address this issue, note that the left-hand side (LHS) of (19) is a concave function of $\alpha_k[n]$, which can be effectively upper-bounded using its first-order Taylor approximation [24]. Following the PCCP framework [25], nonnegative slack variables $\rho_k[n] \ge 0$ are introduced to relax the constraint, allowing the feasible region to expand while gradually reinforcing binary feasibility during successive iterations. Consequently, constraint (19) is replaced with the following convex surrogate expression:

$$(\tilde{\alpha}_k[n])^2 + \alpha_k[n](1 - 2\tilde{\alpha}_k[n]) \le \rho_k[n], \ \forall k, n, \tag{20}$$

where $\tilde{\alpha}_k[n]$ denotes the pickup indicator of the UAV for item k at time slot n obtained from the previous SCA iteration.

To manage the nonconvexity of constraint (9), it is alternatively reformulated as

$$\alpha_k[n] \le \frac{R_k^2 + \varepsilon}{\|\mathbf{c}[n] - \mathbf{c}_k\|^2 + \varepsilon}, \tag{21}$$

where $\varepsilon > 0$ is a constant introduced to avoid division by zero. Although this transformation preserves the original nonconvex structure, the right-hand side (RHS) is a convex function

of $\|\mathbf{c}[n]-\mathbf{c}_k\|^2+\varepsilon$. To obtain a tractable representation, a first-order Taylor approximation is applied at a local point $\tilde{\mathbf{c}}[n]$, yielding the following convex lower-bound form:

$$\alpha_k[n] \le \frac{R_k^2+\varepsilon}{\|\tilde{\mathbf{c}}[n]-\mathbf{c}_k\|^2+\varepsilon} - \frac{R_k^2+\varepsilon}{(\|\tilde{\mathbf{c}}[n]-\mathbf{c}_k\|^2+\varepsilon)^2}\left(\|\mathbf{c}[n]-\mathbf{c}_k\|^2 - \|\tilde{\mathbf{c}}[n]-\mathbf{c}_k\|^2\right),\ \forall k, n\neq N. \quad (22)$$

Applying a similar convexification approach to constraint (10), the following convex set can be obtained.

$$\alpha_k[n] \le \frac{R_k^2+\varepsilon}{\|\tilde{\mathbf{q}}[j]-\mathbf{q}_k\|^2+\varepsilon} - \frac{R_k^2+\varepsilon}{(\|\tilde{\mathbf{q}}[j]-\mathbf{q}_k\|^2+\varepsilon)^2}\left(\|\mathbf{q}[j]-\mathbf{q}_k\|^2 - \|\tilde{\mathbf{q}}[j]-\mathbf{q}_k\|^2\right), \quad \forall k, n\neq N, j\in\{n-1, n+1\}, \quad (23)$$

where $\tilde{\mathbf{q}}[j]$ denotes the horizontal position of the UAV at time slot j obtained from the previous SCA iteration.

To convexify constraint (16), we leverage the fact that $r_l[n]$ is a convex function with respect to $\|\mathbf{c}[n]-\mathbf{c}_l\|^2$. Based on this property, a first-order Taylor approximation around the previous iteration point $\tilde{\mathbf{c}}[n]$ is applied to obtain a linear lower bound of $r_l[n]$, expressed as

$$\begin{aligned} r_l[n] &\ge -\tilde{A}_l[n](\|\mathbf{c}[n]-\mathbf{c}_l\|^2 - \|\tilde{\mathbf{c}}[n]-\mathbf{c}_l\|^2) + \log_2\left(1+\frac{\mu_0 p_{\text{tx}}}{\sigma^2\|\tilde{\mathbf{c}}[n]-\mathbf{c}_l\|^2}\right) \\ &\triangleq \bar{r}_l[n], \end{aligned} \quad (24)$$

where $\tilde{A}_l[n]$ is represented by

$$\tilde{A}_l[n] = \frac{\log_2(e)\mu_0 p_{\text{tx}}}{\mu_0 p_{\text{tx}}\|\tilde{\mathbf{c}}[n]-\mathbf{c}_l\|^2 + \sigma^2\|\tilde{\mathbf{c}}[n]-\mathbf{c}_l\|^4}. \quad (25)$$

By replacing $r_l[n]$ in (16) with its convex surrogate $\bar{r}_l[n]$, the original nonconvex constraint is reformulated into the following convex inequality:

$$\bar{R}_l = \frac{1}{N}\sum_{n=1}^{N} s_l[n]\bar{r}_l[n] \ge R_{\min},\ \forall l. \quad (26)$$

It should be noted that the above SCA approximations are conservative convex approximations. Specifically, the convexified constraints in (22), (23), and (26) form inner approximations of the corresponding original constraints, since the surrogate functions used in these constraints are constructed as locally tight lower bounds at the previous iteration point. Therefore, satisfying these convexified constraints preserves feasibility with respect to the original pickup-zone and minimum-SE constraints.

Accordingly, R_l in the objective function is also replaced by its convex surrogate $\bar{R}_l$ so that the resulting subproblem becomes fully convex and can be directly solved by standard convex solvers. Based on the relaxed and convexified constraints derived above, the subproblem **(P2-2)** can be reformulated as the following convex optimization problem:

$$\begin{aligned} \textbf{(P2-2')}: \max_{\boldsymbol{\alpha},\mathbf{c},\boldsymbol{\rho}}\ & \sum_{l=1}^{L}\ln(\bar{R}_l) - \nu\mathcal{P}(\boldsymbol{\rho}) \\ \text{subject to}\ & (1),\ (2),\ (4)\text{–}(8),\ (18),\ (20),\ (22),\ (23),\ (26), \end{aligned}$$

where the penalty function is defined as $\mathcal{P}(\boldsymbol{\rho}) = \sum_{k=1}^{K}\sum_{n=1}^{N}\rho_k[n]$ where $\boldsymbol{\rho} \triangleq \{\rho_k[n], \forall k, n\}$. The term $\mathcal{P}(\boldsymbol{\rho})$ penalizes deviations from the binary property of the pickup assignment variables, effectively guiding $\alpha_k[n]$ toward discrete values of 0 or 1. The weighting parameter $\nu > 0$ controls the trade-off between the main optimization objective and the penalty term

in subproblem **(P2-2′)**. When ν is small, the optimization process prioritizes improving the primary objective, which may permit nonzero slack variables $\rho_k[n]$, leading to temporarily relaxed values of $\alpha_k[n]$. As ν increases, the penalty term becomes more dominant, progressively driving $\rho_k[n]$ toward zero and tightening the binary constraint. This continuation strategy ensures a smooth transition from a relaxed problem to a binary-feasible solution, enabling stable convergence of the proposed SCA–PCCP framework while preserving computational efficiency [25].

3.3. Proposed Algorithm

Both subproblems, **(P2-1)** and **(P2-2′)**, are convex with respect to their respective optimization variables. These subproblems can be solved using a convex solver until convergence. The detailed procedure is outlined in Algorithm 1.

Algorithm 1 Proposed Algorithm

Set $r=0$ and initialize $\boldsymbol{s}$, $\boldsymbol{\alpha}$, $\boldsymbol{c}$, $\boldsymbol{\rho}$, ν, $\nu_{\max}$, and $\gamma > 1$
Calculate $\eta^r = \sum_{l=1}^{L} \ln(R_l)$ based on these initial values
repeat
  $r \leftarrow r+1$
  $\eta^{\text{old}} \leftarrow \eta^{r-1}$
  Find $\boldsymbol{s}^r$ by solving **(P2-1)** for given $\{\boldsymbol{s}^{r-1}, \boldsymbol{\alpha}^{r-1}, \boldsymbol{c}^{r-1}, \boldsymbol{\rho}^{r-1}\}$
  Find $\{\boldsymbol{\alpha}^r, \boldsymbol{c}^r, \boldsymbol{\rho}^r\}$ by solving **(P2-2′)** for given $\{\boldsymbol{s}^r, \boldsymbol{\alpha}^{r-1}, \boldsymbol{c}^{r-1}, \boldsymbol{\rho}^{r-1}\}$
  Update $\nu^r = \min\{\gamma\nu^{r-1}, \nu_{\max}\}$
  Calculate $\eta^r = \sum_{l=1}^{L} \ln(R_l) - \nu^r \mathcal{P}(\boldsymbol{\rho}^r)$
until $|\eta^r - \eta^{\text{old}}| \le \epsilon$.

The proposed algorithm follows the standard convergence behavior of SCA/PCCP-based iterative optimization. For a fixed penalty parameter, each convexified subproblem is solved using a locally tight approximation, and the block-coordinate updates improve or maintain the objective value. Since the achievable SE is bounded within the finite flight region, the objective value is also bounded above. Although ν is gradually increased during the PCCP process, it is upper-bounded by $\nu_{\max}$. Once ν reaches $\nu_{\max}$, the objective sequence becomes nondecreasing and converges to a stationary point under the standard SCA/PCCP methods.

According to the worst-case complexity analysis of interior-point methods [24,26], when the number of optimization variables is X, the number of iterations required to obtain an ϵ-accurate solution scales as $\mathcal{O}(\sqrt{X}\log(1/\epsilon))$, and the computational cost per iteration scales as $\mathcal{O}(X^3)$. Therefore, solving one convex subproblem has the worst-case complexity of $\mathcal{O}(X^{3.5}\log(1/\epsilon))$. In Algorithm 1, the scheduling subproblem **(P2-1)** contains scheduling variables over all GNs and time slots, whose size scales as $\mathcal{O}(NL)$. The trajectory-pickup subproblem **(P2-2′)** contains the pickup assignment variables, slack variables, and UAV trajectory variables, whose size scales as $\mathcal{O}(NK+N)$. Hence, the dominant number of optimization variables per SCA-PCCP iteration can be approximated as $X = \mathcal{O}(N(K+L))$. Since Algorithm 1 repeats these convex optimization steps for I iterations until convergence, the total computational complexity is estimated as $\mathcal{O}\big(I(N(K+L))^{3.5}\log(1/\epsilon)\big)$. This implies that the total runtime grows polynomially with the problem size $N(K+L)$, following an order of approximately 3.5. The resulting polynomial complexity indicates that the proposed approach remains computationally tractable for planning-stage optimization over a given flight horizon [27].

4. Performance Evaluation and Discussion

In the performance evaluation, GNs and pickup zones are uniformly distributed within a 500 m × 500 m region. The default simulation parameters are summarized in Table 2 [11–13,15,16]. The total item weight is 28 kg, which is below $W_{\max}$ = 30 kg. Since the UAV

carries all collected items until the end of the mission, the payload feasibility is governed by the cumulative carried weight; hence, the feasible trajectory space becomes restricted or infeasible as the cumulative payload approaches or exceeds $W_{\max}$. The proposed scheme is then compared with the following three baseline schemes.

1. Proposed scheme: The UAV strategy including $\boldsymbol{s}$, $\boldsymbol{\alpha}$, and $\boldsymbol{c}$ are optimized by Algorithm 1.
2. Fixed scheduling scheme: The GNs are served in a predetermined scheduling order, and each GN is assigned an equal-duration time slot for uplink transmission, while the remaining variables are optimized accordingly.
3. Fixed trajectory scheme: The UAV sequentially picks up items along the shortest straight-line paths from the origin to each nearest item at the maximum speed until reaching the last pickup point, and then moves from the last pickup point to the destination by evenly allocating the remaining time slots, during which the scheduling indicator is optimized accordingly.
4. Fixed pickup scheme: The pickup order is determined according to the weight of the items in ascending order, while the remaining variables are optimized accordingly.

The considered baseline schemes are selected to isolate the individual impacts of communication scheduling, trajectory design, and pickup-order optimization. While the benchmark set is not intended to exhaust all possible heuristic designs, it provides focused comparisons that directly evaluate the main components of the proposed joint optimization framework. In the simulations, the UAV trajectory is initialized as a straight-line path from the origin to the destination, the altitude is initialized to the nominal flight altitude H, the pickup variables are initialized as $\alpha_k[n] = 0$, and the scheduling variables are initialized uniformly as $s_l[n] = 1/L$. This simple initialization is used as the starting point for the SCA-PCCP iterations.

Table 2. Parameter Setup.

Description	Value
Number of GNs	$L = 4$
Number of items	$K = 4$
Number of time slots	$N = 150$
Length of time slots	$\delta = 1$ s
Maximum flight speed	$V_{\max} = 30$ m/s
Altitude	$H = 20$ m
Maximum payload capacity	$W_{\max} = 30$ kg
Item weights	$\{w_1, w_2, w_3, w_4\} = \{4, 6, 8, 10\}$ kg
Tolerance for pickup zones	$R_k = 1$ m, $\forall k$
Required time slot for pickup mission	$N_{\text{req}} = 80$
Minimum required SE	$R_{\min} = 4$ bps/Hz
Average channel power gain	$\mu_0 = -30$ dB
Noise power	$\sigma^2 = -100$ dBm
Transmit power of GNs	$p_{\text{tx}} = 30$ dBm
Penalty parameters	$\{\nu^0, \nu_{\max}, \gamma\} = \{100, 10^5, 1.2\}$
Convergence threshold	$\epsilon = 10^{-2}$

Figure 2 depicts the trajectory and resource allocation of the proposed scheme. Specifically, Figure 2a illustrates the optimized horizontal trajectory of the UAV when $N_{\text{req}} = 150$. The origin and destination are marked with blue squares, each pickup zone is represented by an empty circle annotated with its corresponding item weight, and the GNs are denoted by filled circles. To indicate which GN is scheduled at each time slot along the trajectory, different colors are applied to the corresponding segments of the UAV path. As shown,

the UAV sequentially visits every pickup zone to retrieve all items. The corresponding altitude and pickup indicator are shown in the upper subfigure of Figure 2b. Each pickup event is triggered exactly once per item, where the pickup indicator switches to 1 in a strictly binary manner, and the UAV descends to the pickup zone with an accuracy of within R_k = 1 m. In the lower subfigure of Figure 2b, the scheduling indicator also exhibits proper binary behavior; the UAV predominantly allocates uplink communication opportunities to the nearest GN along its trajectory. Notably, because the UAV does not explicitly hover above GN 4, it compensates for its disadvantageous channel condition by allocating a longer scheduling duration to GN 4, which in turn allows all GNs to attain comparable service rates. Finally, it is worth noting that when the pickup slot is sufficiently relaxed (N_{req} = 150), the UAV does not follow a purely straight-line path between pickup zones. Instead, it bends its trajectory slightly toward GNs to improve channel conditions. This detour provides a larger gain in the proportional-fair objective than simply minimizing flight distance, thereby producing the curved trajectory observed in Figure 2a.

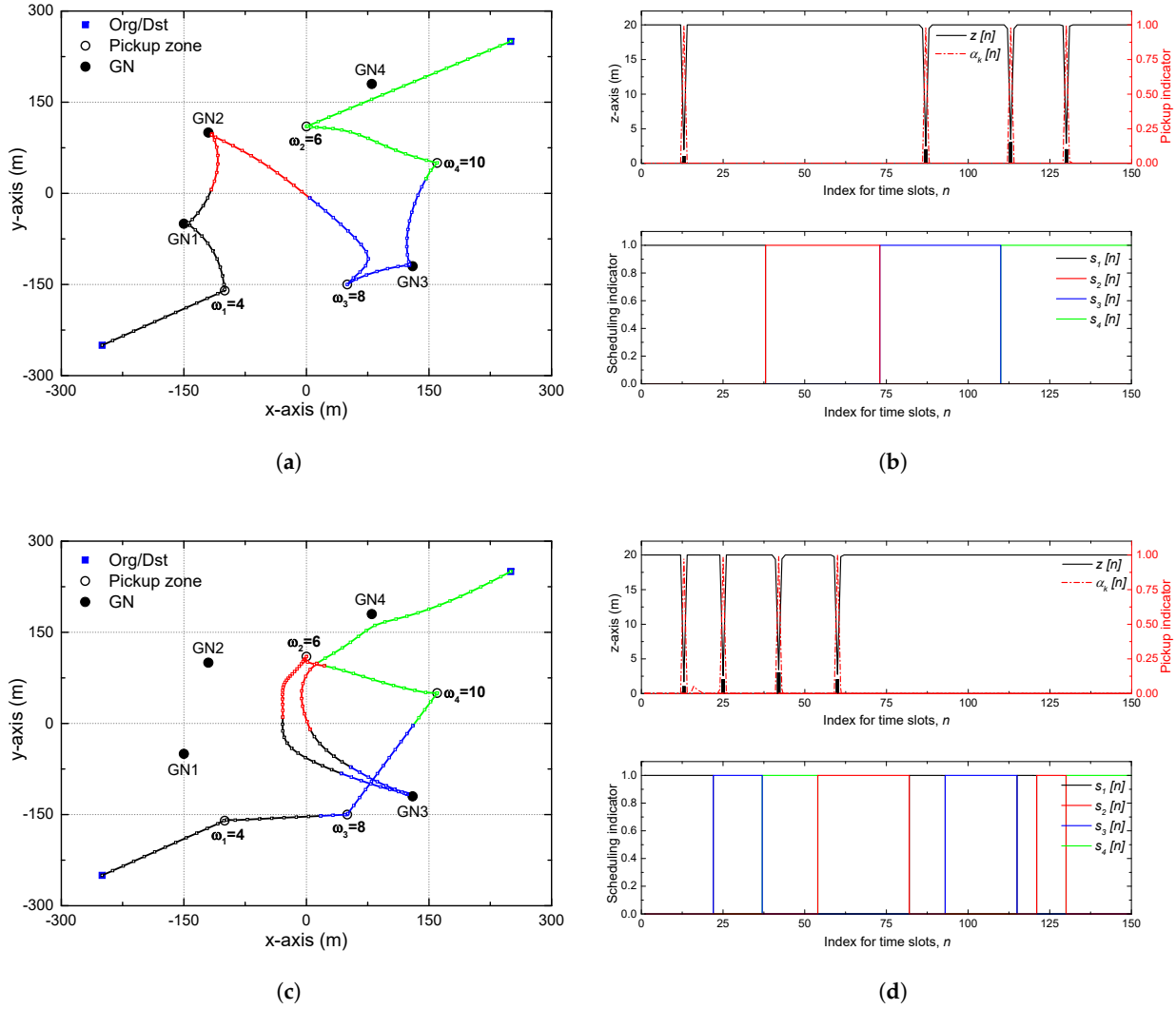


Figure 2. Trajectory and resource allocation of proposed scheme. (**a**) Horizontal trajectory when N_{req} = 150. (**b**) Vertical trajectory and pickup/scheduling indicator when N_{req} = 150. (**c**) Horizontal trajectory when N_{req} = 60. (**d**) Vertical trajectory and pickup/scheduling indicator when N_{req} = 60.

Figure 2c shows the optimized horizontal trajectory when N_{req} = 60, where the UAV is required to complete all item pickups within a much shorter time window. Because the UAV must finish the logistics task early, it cannot afford to visit all GNs individually for commu-

nication service. Nonetheless, to compensate for GN 1 and GN 2, which are not directly visited due to the strict pickup constraint, the UAV deliberately shapes curved segments toward them and schedules uplink transmission at the moments when it passes relatively close to their locations. As observed in the upper subfigure of Figure 2d, the UAV successfully completes every item pickup within the first $n = 60$ time slots, and the pickup indicator switches to 1 in a strictly binary manner for each item. In addition, the altitude trajectory satisfies the pickup altitude constraint precisely, confirming that the UAV descends only within the allowable pickup zones. The lower subfigure of Figure 2d further verifies that the scheduling indicator also maintains binary behavior throughout the mission. The UAV allocates communication opportunities to individual GNs when it becomes geographically closer to them along the trajectory, ensuring that each GN receives service even without the UAV explicitly hovering at every GN location. The binary behavior of the pickup indicators in Figure 2b,d further verifies the effectiveness of the PCCP penalty. Since $\rho_k[n]$ is introduced to relax the binary-enforcing constraint of $\alpha_k[n]$, binary values of $\alpha_k[n]$ indicate that the corresponding relaxation is removed. Therefore, the observed pickup indicators, which take the value 1 only at the selected pickup slots and 0 otherwise, confirm that $\rho_k[n]$ is driven to zero after convergence. In addition to this visual confirmation, the maximum residual slack value after convergence was $\max_{k,n} \rho_k[n] = 0.00084$ in the simulations. This quantitatively confirms that the PCCP penalty drives $\rho_k[n]$ sufficiently close to zero and effectively enforces the binary feasibility of the pickup assignment variables.

Figure 3 evaluates the system performance in terms of PF SE ($\sum_{l=1}^{L} \ln(R_l)$), average SE per GN ($\sum_{l=1}^{L} R_l/L$), and user fairness. Because the PF SE jointly reflects both SE and fairness, we additionally examine its two constituent components to provide deeper insight into how communication efficiency and fairness evolve across different pickup mission requirements (N_{req}). Here, the max–min fairness is adopted as the fairness index, such as $\frac{\min_l R_l}{\max_l R_l}$. As N_{req} increases, the UAV is afforded higher flexibility in jointly performing communication and pickup operations, allowing it to shape its trajectory closer to GNs without sacrificing the logistics constraint. Accordingly, all three performance indicators improve with N_{req}, such that the UAV can achieve high SE for every GN while simultaneously providing fair service across GNs. For the considered parameter ranges, no infeasible case occurred for the proposed scheme. In addition, all final solutions satisfy the minimum SE constraint $R_l \geq R_{\min}$ for every GN. Hence, the performance degradation under a tight pickup deadline is caused by the reduced trajectory and scheduling flexibility, rather than by infeasibility or a violation of the minimum SE constraint. In addition, the proposed method consistently outperforms all baselines over the entire range of N_{req}, highlighting the advantage of optimizing trajectory, pickup scheduling, and communication scheduling in an integrated manner. The fixed scheduling scheme exhibits extremely poor performance when $N_{\text{req}} = 60$ because the pickup-driven trajectory under a tight deadline is incompatible with the predetermined GN scheduling order; only when N_{req} increases does the UAV regain mobility flexibility, enabling the scheme to become feasible again and achieve performance comparable to the other baselines. Moreover, the fixed trajectory scheme yields the lowest performance because the UAV path is predetermined to visit the pickup zones as quickly as possible, leaving only the communication scheduling to be optimized along that path. In contrast, the fixed pickup scheme achieves the highest performance among the baselines because, although the pickup order is predetermined, the pickup timing, trajectory design, and communication scheduling can still be freely optimized. This flexibility enables the UAV to form communication-efficient paths and allocate scheduling opportunities in a balanced manner, leading to superior overall performance compared with the other baseline methods.

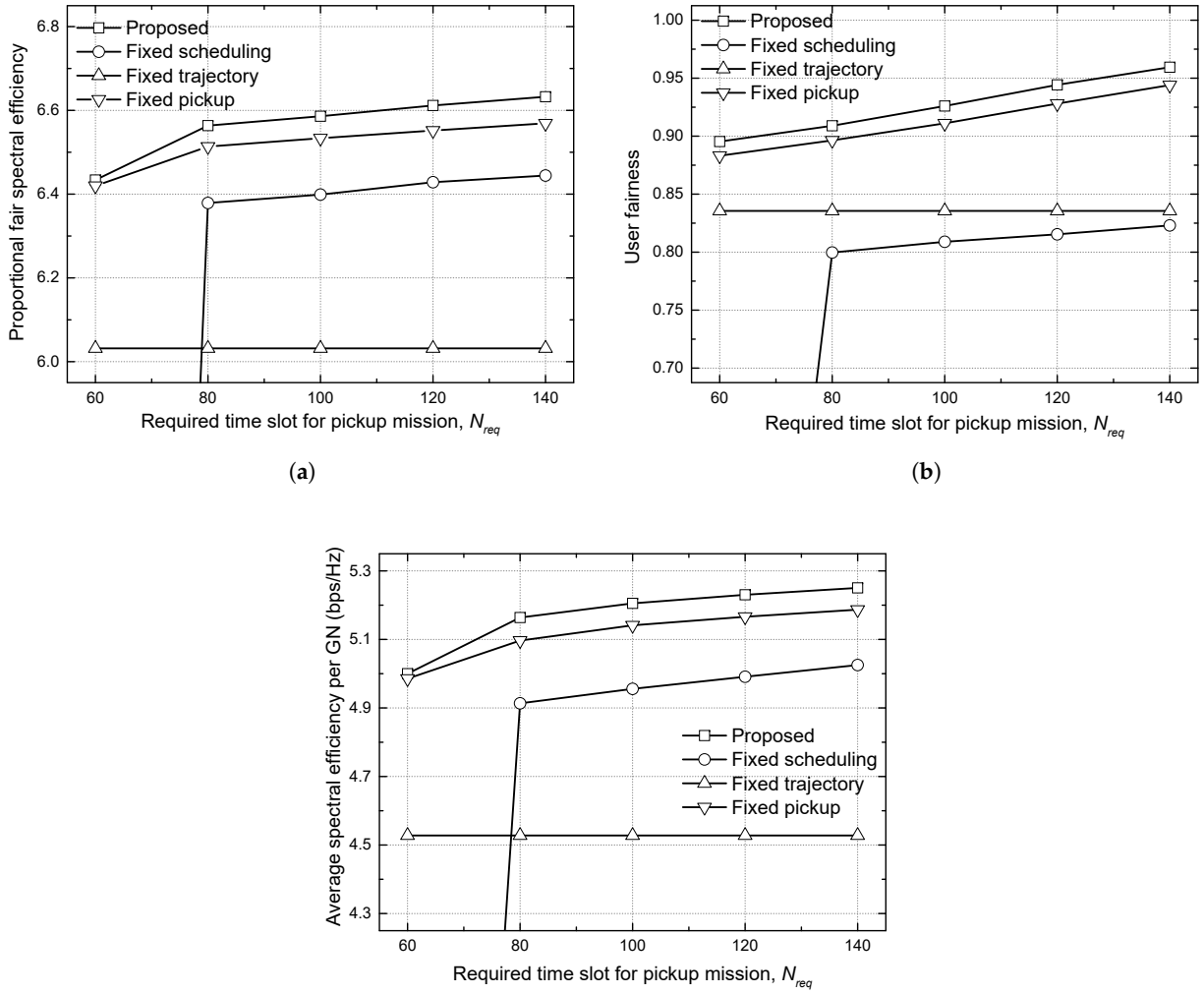


Figure 3. Performance comparisons against N_{req}. (**a**) Proportional fair spectral efficiency. (**b**) User fairness. (**c**) Average spectral efficiency per GN.

Figure 4 compares the performance of different schemes under various system parameters: (a) the number of time slots for flight (N), (b) the minimum required SE ($R_{\min}$), and (c) the maximum flight speed ($V_{\max}$). For all schemes except the fixed trajectory scheme, the performance improves as each parameter increases. Specifically, a larger N provides more time flexibility for the UAV to jointly accommodate both pickup and communication objectives; a larger $R_{\min}$ suppresses low-quality transmissions at long distances and forces the scheduler to allocate more favorable transmission opportunities to weaker GNs. This reduces the SE disparity among GNs and thus enhances the PF SE; and a larger $V_{\max}$ expands the UAV mobility range within a given time slot, enabling more aggressive trajectory shaping toward communication-beneficial regions. Although the underlying mechanisms differ in detail, the common rationale is that increasing any of the three parameters effectively enlarges the optimization search space, allowing the UAV to schedule transmissions at more favorable locations and ultimately boosting the PF objective. In contrast, the fixed trajectory scheme behaves differently because the UAV path is predetermined as a straight line connecting the origin to the pickup zones and then to the destination, leaving only the communication scheduling to be optimized. As N or $V_{\max}$ increases, the UAV reaches the last pickup point earlier and consequently spends a larger fraction of the time slots on

the final segment to the destination, where channel conditions are generally unfavorable. This enlarges the proportion of low-rate transmission periods in the averaging window and thus degrades the PF SE. On the other hand, the performance remains almost constant with respect to $R_{\min}$. Because the UAV cannot reposition itself closer to GNs when the SE requirement becomes more stringent, tightening $R_{\min}$ does not change the communication locations or timing along the fixed path, and therefore the achieved SE stays nearly unaffected. Across all parameter configurations, the proposed scheme consistently achieves the highest PF SE because it jointly optimizes trajectory, pickup timing/sequence, and GN scheduling, and therefore fully leverages the additional degrees of freedom provided by higher N, $R_{\min}$, and $V_{\max}$.

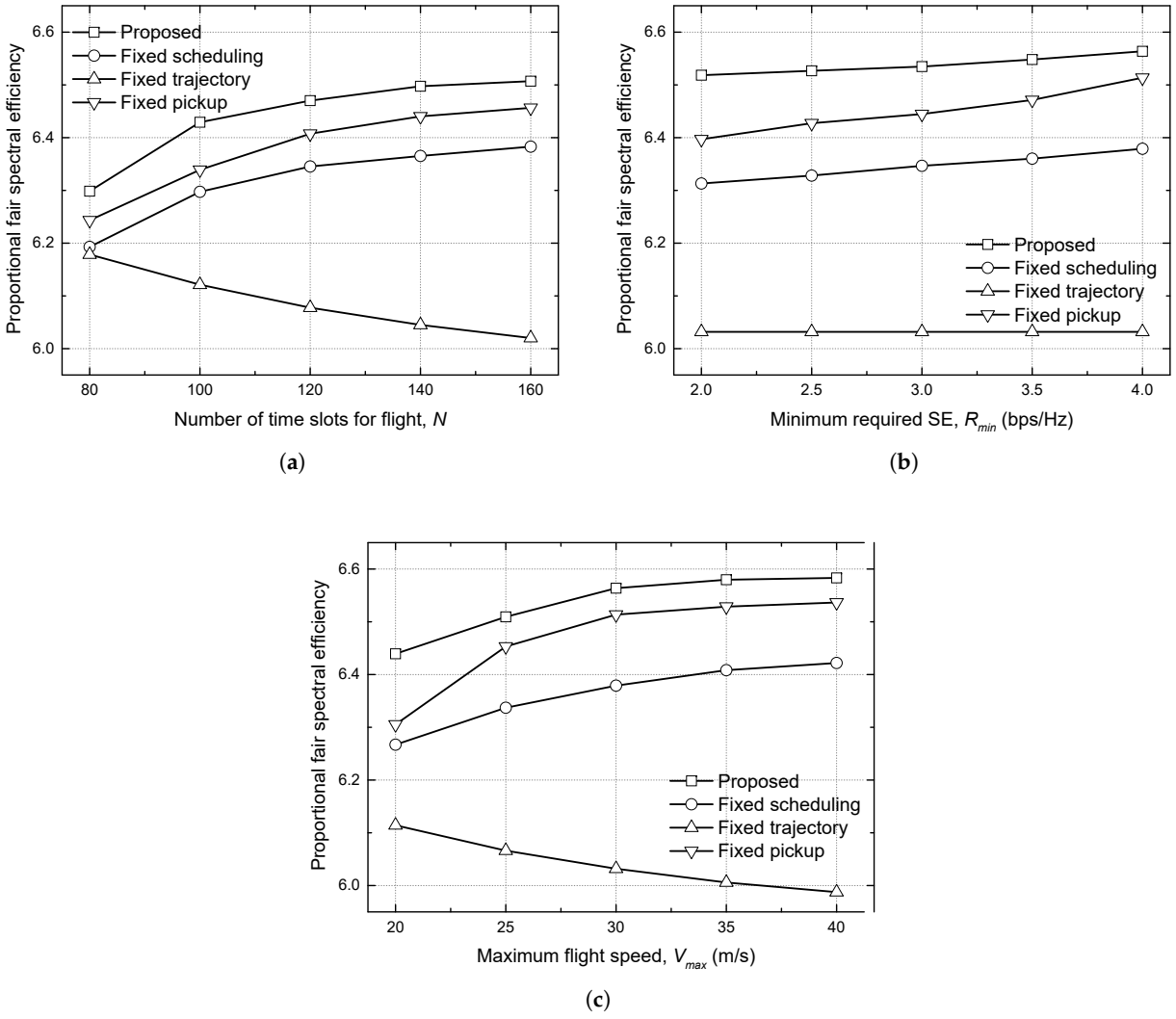


Figure 4. Performance comparisons against various parameters. (**a**) Proportional fair spectral efficiency vs. N. (**b**) Proportional fair spectral efficiency vs. $R_{\min}$. (**c**) Proportional fair spectral efficiency vs. $V_{\max}$.

5. Conclusions

This paper investigated a UAV system that simultaneously provides uplink communication to multiple GNs and performs time-constrained item-pickup missions. Unlike conventional approaches that handle logistics or communication independently, the proposed framework considers the strong coupling among trajectory planning, pickup timing/sequence, and communication scheduling, and jointly optimizes all three components under payload, altitude, and spatial-safety constraints. By integrating SCA and PCCP into

a block-coordinate optimization structure, the proposed algorithm efficiently tackles the mixed-integer nonconvex problem and yields a high-quality feasible solution with polynomial computational complexity. Simulation results demonstrated several key insights. The UAV autonomously bends its trajectory toward communication-beneficial regions while still completing all pickups before the deadline, and dynamically adjusts scheduling to compensate for disadvantaged GNs. The proposed scheme maintained proportional fairness among GNs even under tight mission constraints and exhibited consistent performance advantages over the baselines across various parameter settings. This study focuses on offline mission planning over a given flight horizon, and online adaptation to dynamic environments is not explicitly considered. Future work may extend the proposed framework to online or receding-horizon optimization and incorporate hybrid methods based on artificial intelligence, genetic algorithms, or particle swarm optimization.

Funding: This work was supported by the National Research Foundation of Korea (NRF) grant funded by the Korea government (MSIT) (RS-2025-16065671).

Institutional Review Board Statement: Not applicable.

Informed Consent Statement: Not applicable.

Data Availability Statement: The original contributions presented in this study are included in the article.

Conflicts of Interest: The author declares no conflicts of interest.

References

1. Geraci, G.; Garcia-Rodriguez, A.; Azari, M.M.; Lozano, A.; Mezzavilla, M.; Chatzinotas, S.; Chen, Y.; Rangan, S.; Renzo, M.D. What will the future of UAV cellular communications be? A flight from 5G to 6G. *IEEE Commun. Surv. Tuts.* **2022**, *24*, 1304–1335. [CrossRef]
2. Dissanayaka, D.; Wanasinghe, T.R.; De Silva, O.; Jayasiri, A.; Mann, G.K.I. Review of navigation methods for UAV-based parcel delivery. *IEEE Trans. Autom. Sci. Eng.* **2024**, *21*, 1068–1082. [CrossRef]
3. Seo, J.; Choi, Y.; Jeon, S.-E.; Chae, S.; Hong, J.-P. Learning-based geographic routing for delay-limited multi-hop wireless networks. *IEEE Sens. J.* **2024**, *24*, 42163–42171. [CrossRef]
4. Luu, V.C.; Hong, J.-P. GNN-based meta-learning approach for adaptive power control in dynamic D2D communications. *IEEE Trans. Veh. Technol.* **2024**, *73*, 5982–5987. [CrossRef]
5. Hong, J.-P.; Park, J.; Shin, W.; Baek, S. Spectral efficient resource allocation for URLLC in distributed antenna systems. *IEEE Trans. Veh. Technol.* **2020**, *69*, 15057–15067. [CrossRef]
6. Evgenidis, S.P.; Karapantsios, T.D.; Kostoglou, M. Bubble size effect on electrical signal fluctuations in flow of sub-millimeter bubbles at low void fractions: A simulation study. *Exp. Comput. Multiph. Flow* **2025**, *7*, 308–322. [CrossRef]
7. Wu, Q.; Zeng, Y.; Zhang, R. Joint trajectory and communication design for multi-UAV enabled wireless networks. *IEEE Trans. Wirel. Commun.* **2018**, *17*, 2109–2121. [CrossRef]
8. Heo, K.; Park, G.; Lee, K. Joint optimization of UAV trajectory and communication resources with complete avoidance of no-fly-zones. *IEEE Trans. Intell. Transp. Syst.* **2024**, *25*, 14259–14265. [CrossRef]
9. Zeng, Y.; Xu, J.; Zhang, R. Energy minimization for wireless communication with rotary-wing UAV. *IEEE Trans. Wirel. Commun.* **2019**, *18*, 2329–2345. [CrossRef]
10. Gu, J.; Wang, H.; Ding, G.; Xu, Y.; Xue, Z.; Zhou, H. Energy-constrained completion time minimization in UAV-enabled Internet of Things. *IEEE Internet Things J.* **2020**, *7*, 5491–5503. [CrossRef]
11. Park, G.; Heo, K.; Lee, W.; Lee, K. UAV-assisted wireless-powered two-way communications. *IEEE Trans. Intell. Transp. Syst.* **2024**, *25*, 2641–2655. [CrossRef]
12. Kim, C.; Choi, H.-H.; Lee, K. Joint optimization of trajectory and resource allocation for multi-UAV-enabled wireless-powered communication networks. *IEEE Trans. Commun.* **2024**, *72*, 5752–5764. [CrossRef]
13. Heo, K.; Choi, H.-H.; Lee, K. Joint trajectory and resource optimization for UAV-assisted SWIPT systems: A comparative study of linear and nonlinear energy harvesting models. *IEEE Internet Things J.* **2024**, *11*, 40293–40305. [CrossRef]
14. Yi, P.; Zhu, L.; Xiao, Z.; Zhang, R.; Han, Z.; Xia, X.-G. Trajectory design and resource allocation for multi-UAV communications under blockage-aware channel model. *IEEE Trans. Wirel. Commun.* **2024**, *72*, 2324–2338. [CrossRef]

15. Lee, H.; Eom, S.; Park, J.; Lee, I. UAV-aided secure communications with cooperative jamming. *IEEE Trans. Veh. Technol.* **2018**, *67*, 9385–9392. [CrossRef]
16. Heo, K.; Lee, W.; Lee, K. UAV-assisted wireless-powered secure communications: Integration of optimization and deep learning. *IEEE Trans. Wirel. Commun.* **2024**, *23*, 10530–10545. [CrossRef]
17. Dorling, K.; Heinrichs, J.; Messier, G.G.; Magierowski, S. Vehicle routing problems for drone delivery. *IEEE Trans. Syst. Man Cybern. Syst.* **2017**, *47*, 70–85. [CrossRef]
18. Huang, H.; Hu, C.; Zhu, J.; Wu, M.; Malekian, R. Stochastic task scheduling in UAV-based intelligent on-demand meal delivery system. *IEEE Trans. Intell. Transp. Syst.* **2022**, *23*, 13040–13054. [CrossRef]
19. Park G.; Lee, W.; Lee, K. 3D multi-trajectory and pick-up optimization of UAV for minimizing delivery time with weight restriction. *IEEE Trans. Intell. Transp. Syst.* **2024**, *25*, 17562–17573. [CrossRef]
20. Wen, W.; Luo, K.; Liu, L.; Zhang, Y.; Jia, Y. Joint trajectory and pick-up design for UAV-assisted item delivery under no-fly zone constraints. *IEEE Trans. Veh. Technol.* **2023**, *72*, 2587–2592. [CrossRef]
21. Kuru, K.; Ansell, D.; Khan, W.; Yetgin, H. Analysis and optimization of unmanned aerial vehicle swarms in logistics: An intelligent delivery platform. *IEEE Access* **2019**, *7*, 15804–15831. [CrossRef]
22. Lee, K.; Jo, O.; Cho, D.-H. Cooperative resource allocation for guaranteeing intercell fairness in femtocell networks. *IEEE Commun. Lett.* **2011**, *15*, 214–216. [CrossRef]
23. Grant, M.; Boyd, S. CVX: MATLAB Software for Disciplined Convex Programming, Version 2.1. 2017. Available online: http://cvxr.com/cvx (accessed on 20 May 2026).
24. Boyd, S.; Vandenberghe, L. *Convex Optimization*; Cambridge University Press: Cambridge, UK, 2004.
25. Lipp, T.; Boyd, S. Variations and extension of the convex–concave procedure. *Optim. Eng.* **2016**, *17*, 263–287. [CrossRef]
26. Ben-Tal, A.; Nemirovski, A. *Lectures on Modern Convex Optimization: Analysis, Algorithms, and Engineering Applications*; SIAM: Philadelphia, PA, USA, 2001.
27. Leiserson, C.E.; Rivest, R.L.; Cormen, T.H.; Stein, C. *Introduction to Algorithms*; MIT Press: Cambridge, MA, USA, 2001.

Disclaimer/Publisher's Note: The statements, opinions and data contained in all publications are solely those of the individual author(s) and contributor(s) and not of MDPI and/or the editor(s). MDPI and/or the editor(s) disclaim responsibility for any injury to people or property resulting from any ideas, methods, instructions or products referred to in the content.